IEEE Access
Multidisciplinary | Rapid Review | Open Access Journal

Received September 5, 2018, accepted October 5, 2018, date of publication October 17, 2018, date of current version November 14, 2018.

Digital Object Identifier 10.1109/ACCESS.2018.2876552

Achieving Efficient Data Collection in Heterogeneous Sensing WSNs

XINGYU HE[1,2], SHUAI LIU[2], GUISONG YANG[2,3], AND NAIXUE XIONG[4]

[1]Public Experiment Center, University of Shanghai for Science and Technology, Shanghai 200093, China
[2]School of Optical-Electrical and Computer Engineering, University of Shanghai for Science and Technology, Shanghai 200093, China
[3]Shanghai Key Laboratory of Modern Optical Systems, Shanghai 20093, China
[4]Department of Mathematics and Computer Science, Northeastern State University, Tahlequah, OK 74464, USA

Corresponding author: Guisong Yang (gsyang@usst.edu.cn)

This work was supported in part by the National Natural Science Foundation of China under Grant 61602305, Grant 61802257, and Grant 61572325 and in part by the Natural Science Foundation of Shanghai under Grant 18ZR1426000.

ABSTRACT Nowadays, many applications of heterogeneous sensing wireless sensor networks (WSNs) employ more than one type of sensor nodes to acquire a variety of sensing data sources, which brings the dynamic diversity of generated data amount among different network regions. To adapt to that diversity and improve the data gathering efficiency, this paper first analyzes and models the diversity of generated data amount according to the diversities of data generating rate and operating mode among nodes and then proposes a data gathering scheme with a mobile sink. In the scheme, the movement trajectory for the mobile sink is determined by using Hilbert space-filling curve and adjusted dynamically based on the change of data amounts generated in different network regions. A hybrid routing method is also proposed to further reduce the network energy consumption. The simulation results show that the proposed data gathering scheme not only has effective performances on a promoting packet delivery ratio and reducing average energy consumption rate but also has great adaptability to the heterogeneous sensing WSNs.

INDEX TERMS Heterogeneous sensing, movement trajectory, Hilbert space-filling curve, hybrid routing.

I. INTRODUCTION

With the development of micro-electromechanical systems and wireless network technologies, tiny and low-power network nodes equipped with diverse sensors have been implemented in recent years, Wireless Sensor Networks (WSNs) so become an important way for people to interact with the physical world, and also turn into one of the supporting technologies in the mainstream applications of Internet of Things (IOT) such as environmental monitoring, healthcare data collection, military detection and geological exploration [1]. In WSNs, each sensor node has limited computing ability, transmission range, memory capacity, and battery life, and the sensing data of each node needs to be gathered to the sink node and then transmitted to the data center.

In WSNs with static sinks, the nodes closer to the sink generally consume more energy for their heavier forwarding burden, and the unbalanced energy consumption causes the hot-spot issues [2], which affects the network connectivity and brings the network partition problem, thereby reducing the entire network lifetime.

To deal with the drawback caused by using the static sink in WSNs, the data gathering schemes based on mobile sinks are proposed and attract increasingly attention in recent years [3]. In these schemes, the mobile sinks move and adopt different kinds of mobility patterns (pre-defined, uncontrolled, or controlled) to collect data from the stationary sensor nodes, which is beneficial for balancing energy consumption to some extent.

Further, in order to plan the movement trajectories for mobile sink(s) in WSNs, the concept of space-filling curve has been introduced. By following the space-filling curve, a mobile sink can traverse all regions in its network. A method to construct the sink trajectory by using Hilbert space-filling curves has been proposed [4]. The method can change the curve orders of Hilbert space-filling curves for adapting to the diversity of node density among different network regions, but, it lacks the adaptability to the diversities of other factors in the heterogeneous sensing WSNs such as data generating rate and operating mode. For example, the modern healthcare information system could be a heterogeneous sensing network, in which, wearable sensing nodes could have different

data generating rates and also could switch their operating modes dynamically according to their working and sleeping schedule tables, thus the data amount generated in a network region may change dynamically and which is not only related to the node density change of the region.

As the sensor cloud system brings new computation paradigms to WSNs in providing users with data collection services [5] and the network interoperability [6], the data gathering schemes in the heterogeneous sensing WSNs become more and more important.

In order to achieve a high data gathering efficiency in the heterogeneous sensing WSNs, in this work, firstly, the diversity of generated data amount among different network regions is modeled by analyzing the diversities of data generating rate and operating mode among nodes, then a data gathering scheme is proposed for the network with a mobile sink following a controlled movement trajectory, in which the sink trajectory is determined by using the Hilbert space-filling curve and can be adjusted dynamically according to the change of the generated data amount in each network region.

The movement trajectory construction for the mobile sink includes two phases, the initializing phase and the data gathering phase. In the initializing phase, the network is divided into cells having an identical size based on both the network size and the maximum transmission range of nodes, and an initial movement trajectory for the mobile sink is constructed by filling the Hilbert curves in the cells.

After the initializing phase, the network steps into the data gathering phase where the data gathering is carried out in rounds. In each round, the mobile sink moves along its current trajectory which is formed according to the data amount in each cell in the previous round, to collect the sensing data generated in the previous round, and to form its movement trajectory for the next round by merging the adjacent cells with small data amounts in current round together, and dividing the cell with large data amount in current round into sub-cells, then updating the curve orders of the Hilbert space-filling curves in the new formed cells.

The main contributions of this work can be summarized as follows:

1. The diversity of generated data amount among different network regions in the heterogeneous sensing WSNs is modeled by analyzing the diversities of data generating rate and operating mode among nodes.

2. A data gathering scheme is proposed to construct the movement trajectory for the mobile sink by using the Hilbert space-filling curve, and adjust the trajectory dynamically according to the change of data amount generated in different network regions.

3. A hybrid routing method, which supports both single-hop transmission mode and cluster mode, is designed to further improve the energy efficiency of sensor nodes.

The rest of this work is organized as follows: in Section II, the related work is introduced; in Section III, the network model is defined; Section IV presents the proposed data gathering scheme in detail; the performance evaluation to the proposed scheme is shown in Section V, and our work is concluded in Section VI.

II. RELATED WORK

Since the mobile sink is superior to the static sink in balancing energy consumption of WSNs, the issue of how to take full advantages of the mobile sink for achieving high flexibility and energy efficiency has attracted increasingly attention from the research community to the industry where much fundamental work has been done. Many studies concentrate on planning the mobility pattern of the mobile sink, because it can affect the energy efficiency and network performance. And, the mobility patterns of the mobile sink in these studies can be roughly classified into three kinds, which are the pre-defined mobility pattern, the uncontrolled (or random) mobility pattern and the controlled mobility pattern.

In the first category, the mobile sink moves along a pre-defined movement trajectory to gather the sensing data from all nodes in network. Wichmann and Korkmaz [7] proposed a smooth path construction algorithm for one or more mobile sinks, which uses the faster and motion-constrained mobile sinks to reduce the collection delay. Viana and Amorim [8] designed a pre-defined trajectory based on a space-filling curve for the mobile sink to increase the packet delivery ratio. Ghafoor *et al.* [9] proposed a novel method to construct the mobile sink trajectory based on the Hilbert space-filling curve, in which both the network size and node density of the whole network are taken into consideration to make the trajectory more flexible. However, this method cannot deal with the network with uneven node density distribution. To solve this problem, an adjustable trajectory design method [4] has been proposed, in which the node density of each network region is taken into account to adjust the sink trajectory. Wang *et al.* [10] proposed an energy-efficient cluster-based route adjustment method, in which the mobile sink adopts the pre-defined mobility and its route is adjusted according to its location to prolong the network lifetime. Mehrabi and Kim [11] proposed an online centralized algorithm to increase the throughput in energy harvesting WSNs with a mobile sink using a pre-defined movement trajectory, which considers both the heterogeneous duration and the effectiveness of sensors in each time slot.

In the second category, the mobile sink moves uncontrollably or randomly, and the sensing data are delivered by tracking the location of the mobile sink. Kinalis *et al.* [12] proposed a data gathering scheme using the mobile sink with probabilistic movement trajectory to improve the energy-latency trade-offs, in which the sink uses a biased random movement trajectory favoring the less visited regions. Liu *et al.* [13] analyzed an uncontrolled mobility pattern of multiple mobile sinks for reducing control overheads and prolonging the network lifetime. Yang *et al.* [14] proposed a sink tracking method called Detour-Aware Mobile Sink Tracking (DAMST), in which mobile sinks are tracked by analyzing their movement angle changes to further cut down the overheads and increase the energy efficiency.

Yang *et al.* [15] proposed a data collection scheme based on social properties and uncontrolled sink mobility. In the scheme, the network is divided into clusters and these clusters are classified into biased and unbiased clusters according to the staying probabilities of the sink, in addition, a biased loop is constructed to disseminate the location of the mobile sink so that every cluster can track the mobile sink in time. Sharma *et al.* [16] proposed a routing protocol for the WSNs with a mobile sink moving randomly, in which, the rendezvous-region is introduced and a tree is constructed, the sensor nodes can transmit their data via the tree and track the mobile sink's location from the tree to upload the data to the sink directly.

In the third category, the movement trajectory for the mobile sink is neither pre-defined nor uncontrolled, and it is determined by some parameters of the network. Wang *et al.* [17] proposed a sink relocation method to extend the network lifetime of WSNs, in which the sink trajectory as well as the sensor nodes' transmission range are adjusted according to the residual battery of sensor nodes. He *et al.* [18] proposed a combine-skip-substitute scheme to schedule the movement of the mobile sink by solving the traveling salesman problem, where the data collection latency is mainly focused, and the multi-rate wireless communication is adopted to further reduce the latency. Kaswan *et al.* [19] proposed an efficient trajectory design method based on Rendezvous Points (RPs) to achieve delay bound data gathering. Zhu *et al.* [20] proposed a greedy scanning data collection strategy, in which, both the cluster algorithm and the controlled mobile movement trajectory for the mobile sink are used, and the sensing data are relayed by the cluster heads tracking the location of the mobile sink. Zhu *et al.* [21] proposed tree-cluster based data gathering algorithm for WSNs to prolong the network lifetime. Salarian *et al.* [22] proposed a Weighted Rendezvous Planning (WRP) method for selecting the trajectories for mobile sink among the Rendezvous Points (RPs), in which the mobile sink only visits the RPs instead of all the nodes and the sink trajectory is acquired by a heuristic algorithm. Rao and Biswas [23] proposed a novel data gathering solution for non-real-time applications, in which nodes determine the movement trajectory of mobile sink cooperatively to optimize delay and energy in data collection. Bi *et al.* [24] provided a method to determine the movement trajectory of the mobile sink according to the nodes' residual energy, so that the energy consumption among sensor nodes is balanced and the network lifetime is prolonged. Ma *et al.* [25] proposed a data gathering scheme by using one or more Mobile Collectors (M-collectors), in which the M-collector needs to follow the constraints about distance or time, collect the sensing data from the sensor nodes directly and relay them to the sink by single-hop transmission.

From above, it can be found that, the pre-defined sink trajectory lacks flexibility and adaptability, and the random sink trajectory has great transmission uncertainty which is adverse to the promotion of packet delivery ratio and also may bring great overhead to nodes on tracking the mobile sink. In view of these problems, we propose a data gathering scheme which uses Hilbert space-filling curve to construct the movement trajectory for the mobile sink and also can adjust the trajectory dynamically according to the change of data amounts in different network regions. In our scheme, the sink trajectory is adjusted in a controlled manner, which not only has adaptability but also contributes to both of the reduction of energy consumption rate and the promotion of packet delivery ratio.

III. NETWORK MODEL

In this work, location-aware nodes equipped with divers sensors are deployed in a square network with side length L. Each node has limited initial energy E and maximum transmission range r_{max}, and can use the GPS-free localization method [26] to acquire its location.

A. MOBILE SINK AND CELL AGENT (CA)

To guarantee the full coverage of the network and achieve efficient data gathering, the network is divided into cells, and the cell that does not contain any sub-cell is called the B-cell. In each B-cell, a Cell Agent (CA) is elected periodically to be responsible for collecting the parameters and the sensing data of the nodes in this B-cell.

In our network model, a mobile sink is used to traverse the cells with a constant speed v_0 starting from the bottom left of the network and gather the collected information of the CAs. Specifically, in each round of the data gathering, the mobile sink needs to traverse the centers of all B-cells in the network once and only once.

The mobile sink is also responsible to broadcast the CA election message which includes a dynamic energy threshold (the energy threshold decreases with time) to the nodes in each B-cell. And in the CA election of a B-cell, a node which is closest to the center of the B-cell is elected from the nodes in the B-cell whose residual energy are beyond the dynamic energy threshold included in their received CA election messages, as the CA of the B-cell.

B. HILBERT SPACE-FILLING CURVE AND THE METHOD FOR NAMING CELLS

In this work, the Hilbert space-filling curve [27] proposed by Hilbert in 1891 is used as the basis to divide cells and construct the movement trajectory for the mobile sink. The *1*-order, *2*-order and *3*-order Hilbert curves are shown in Fig. 1.

As a matter of fact, besides the Hilbert curve, there are still many other space-filling curves. The comparison among the Z-curve, gray-coded curve and Hilbert curve has been made [28], the results show that the Hilbert curve outperforms the others in the properties of clustering and locality, which is the main reason why we use it in this work.

If the Hilbert curve is used in a two-dimension network, the network could be divided into N identical cells (e.g. 2×2, 4×4, 8×8) and the number of the cells N is related to the order k of the Hilbert curve, the relation holds $N = 4^k$.

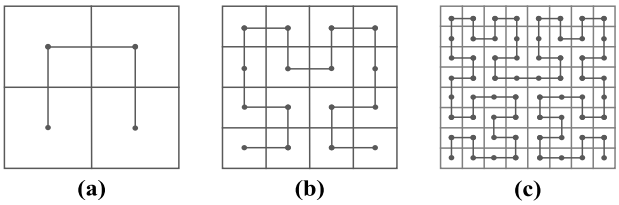

FIGURE 1. Hilbert space-filling curves: (a) *1*-order curve; (b) *2*-order curve; and (c) *3*-order curve.

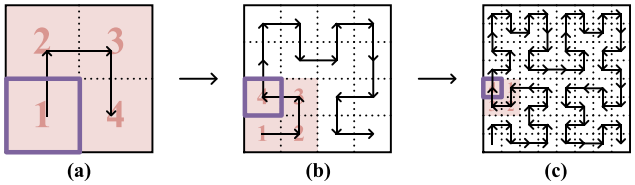

FIGURE 2. Cells in different levels: (a) level-*1* cells with *1*-order Hilbert curve; (b) level-*2* cells with *2*-order Hilbert curve, and (c) level-*3* cells with *3*-order Hilbert curve.

To simplify the discussion, we define the B-cell filled with a k-order Hilbert curve as the level-k cell. The Hilbert curve is constructed recursively. A k-order curve ($k>1$) can be obtained by dividing each level-$k-1$ cell into four identical sub-cells and filling each of the sub-cells with the *1*-order curve, which can be shown by the change from Fig. 1(a) to Fig. 1(b) or from Fig. 1(b) to Fig. 1(c).

Fig. 2 shows an example for illustrating how to name the cells in the network. As shown in Fig. 2(a), the Hilbert curve order is 1, the whole network is divided into four cells, we name these four level-*1* cells by *Ci* (i=*1, 2, 3, 4*), where i represents the sequence in which the mobile sink traverses the four level-*1* cells, for instance, the cell in the purple frame in Fig. 2(a) is named *C1* which is the first cell traversed by the mobile sink. As shown in Fig. 2(b), the Hilbert curve order is increased by 1 (*2*-order Hilbert curve), each level-*1* cell is further divided into four level-*2* cells, we name these level-*2* cells by *Ci-j* ($i, j = 1, 2, 3, 4$), where i is the identification of level-*1* parent cells, and j represents the sequence in which the mobile sink traverses the four level-*2* cells in each level-*1* parent cell, for instance, the cell in the purple frame in Fig. 2(b) is named *C1-4*. Similarly, the level-*3* cells divided from the level-*2* cells are named by *Ci-j-k*, for instance, the cell in the purple frame in Fig. 2(c) is named *C1-4-4*. By the above simple method, every cell in the network can be named.

The level of a cell can be inferred from its name. For example, a cell's name is *C2-3-3*, it can be deduced that, this cell is a level-*3* cell whose parent cells are level-*2* cell *C2-3* and level-*1* cell *C2*.

C. DATA GENERATING RATE AND OPERATING MODE

In this work, the data amounts generated in different network regions may differ and the data amount in a region may also change with time dynamically. The two main factors for this difference and change are: 1) the nodes equipped with different sensors have different data generating rates; 2) the nodes can switch their operating modes during different time periods according to their own schedule tables.

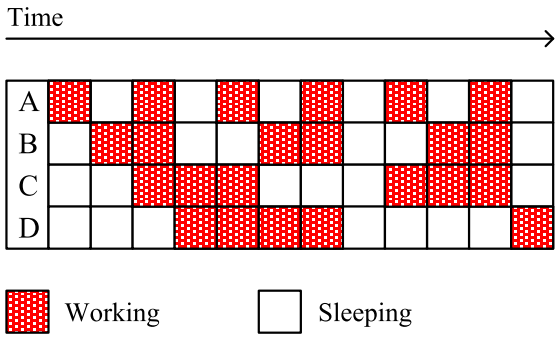

FIGURE 3. An example of schedule tables for four different nodes (A, B, C, and D).

For a node N_i with j different sensors, its data generating rate $R(N_i)$ can be calculated by (1).

$$R(N_i) = \sum^{j} (f_{\mathrm{m}} \times g_{\mathrm{m}}) \tag{1}$$

In (1), the data generating rate $R(N_i)$ is determined by the sampling rate of each sensor of N_i (denoted by f_m, m is the identification of sensors), the resolution of each sensor of N_i (denoted by g_m), and the total number of sensors of N_i (denoted by j). The sampling rate of a sensor determines how many samples it can get from its source per unit time, while the resolution of a sensor determines the size of its sample.

Each node could schedule its working time and sleeping time by its own schedule table, in other words, it can be in different operating modes at different time periods through the whole data gathering process. And consequently, the data amount generated by the same node could also be different during different data gathering rounds. Fig. 3 gives an example to show the schedule tables for four different nodes.

In this work, the basic data gathering unit is B-cell, and we use symbol *Cb* to represent any one of the B-cells. In a data gathering round, the generated data amount in a B-cell could be determined by the data generating rates and the operating modes of all nodes in it jointly. Therefore, the generated data amount in a B-cell *Cb* in a round is denoted by $DS(Cb)$ and it can be calculated as follows:

$$DS(Cb) = \sum_{i=1}^{n} (R(N_i) \times T_{work\_i}) \tag{2}$$

Where n is the number of nodes in *Cb*, $R(N_i)$ is the data generating rate of node N_i in *Cb*, and T_{work_i} is the working time of node N_i in this round.

D. ENERGY MODEL

In this work, we only consider the energy consumption on communication and adopt the free-space channel model [29]. The energy consumption on communication of each node

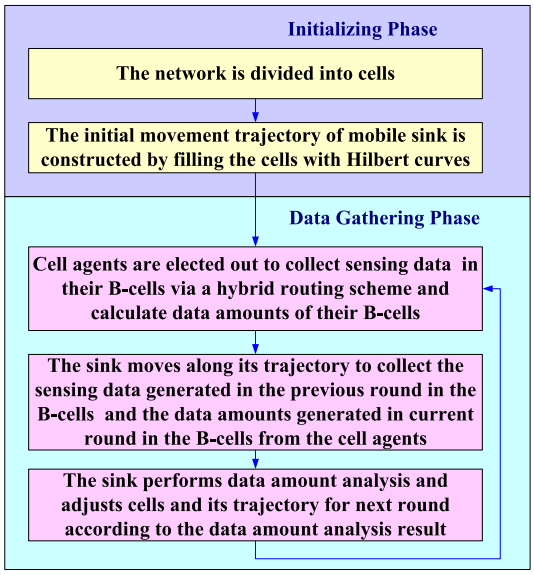

FIGURE 4. Two phases of the movement trajectory construction for the mobile sink.

includes two parts: the transmitting energy and the receiving energy. Let ε_{fs} be the energy required by the amplifier in free-space channel, α_{tx} and α_{rx} be the energy consumed during transmitting and receiving per bit respectively. The transmitting energy consumed by node N_i when it transmits β bits data to node N_j can be calculated as follows:

$$E_{tx}(i,j) = (\alpha_{tx} + \varepsilon_{fs} D^2_{(i,j)})\beta \tag{3}$$

Where $D_{(i,j)}$ is the distance between node N_i and node N_j. The receiving energy consumed by node N_j that receives β bits data from N_i can be calculated as follows:

$$E_{rx}(i,j) = \alpha_{rx}\beta \tag{4}$$

The above energy model is used in all kinds of communication behaviors in this work such as the election of CA and the hybrid routing scheme for collecting sensing data.

IV. MOVEMENT TRAJECTORY CONSTRUCTION AND ROUTING METHOD

In this work, the movement trajectory construction for the mobile sink consists of two phases: the initializing phase and the data gathering phase, which are shown in Fig. 4. In the initializing phase, the network is divided into cells and the initial movement trajectory for the mobile sink is constructed. The data gathering phase is performed in rounds. In each round, CAs are elected out to collect sensing data and calculate data amounts in their B-cells, the mobile sink moves along its current trajectory to collect the sensing data generated in the previous round and the data amount generated in current round in each B-cell from CAs, performs data amount analysis and adjusts cells and its trajectory for the next round according to the analysis result.

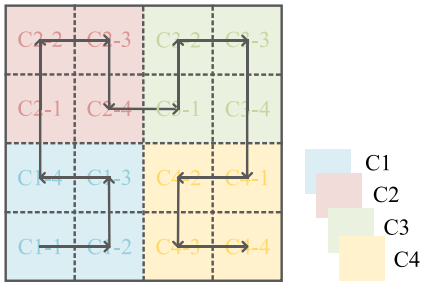

FIGURE 5. An example of sink trajectory ($k = 2$, the number of B-cells is 16).

A. THE INITIALIZING PHASE

In this phase, firstly, the network is divided into B-cells by using the Hilbert curve. To obtain the full coverage of the network, both the network side length L and the maximum transmission range of nodes r_{max} are taken into consideration in calculating a proper Hilbert curve order k. The order k of the Hilbert curve that can cover the network can be calculated by (5).

$$k = \left\lceil \log_2 \left\{ \frac{\sqrt{2}L}{r_{\max}} \right\} \right\rceil \tag{5}$$

After obtaining the proper order k, the network is divided into 4^k B-cells, and the initial movement trajectory for the mobile sink can be constructed to be a k-order Hilbert curve which can traverse the centers of all the 4^k B-cells. For example, the trajectory constructed by a 2-order Hilbert space-filling curve is shown in Fig. 5.

Then, the mobile sink moves along the initial trajectory to disseminate the network location information (i.e. the coordinates of the network center (x_0, y_0), the side length of the network L) and the CA election message to all nodes.

B. THE DATA GATHERING PHASE

After initialization, the network steps into the data gathering phase. The data gathering process is carried out in rounds. And in each round, the mobile sink needs to construct its trajectory for the next round by adjusting its current trajectory according to the data amount change in each B-cell, so that it can adapt to the real time network change and achieve better data gathering efficiency.

1) DATA AMOUNT ANALYSIS

At the beginning of each data gathering round, each CA collects the data generating rate of each node in its B-cell in current round, and calculates the data amount generated in current round in its B-cell. When the mobile sink traverses a B-cell, the CA in this B-cell will send both the sensing data which it has collected in the previous round and the data amount in this B-cell in the current round to the sink.

In a B-cell, the data amount generated in the current round will influence the sink trajectory in the next round. The greater data amount a cell generates in the current round,

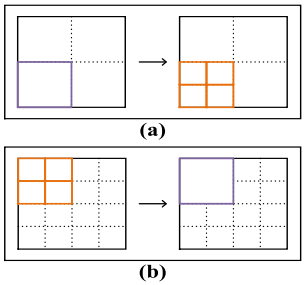

FIGURE 6. Dividing and merging of the B-cell(s): (a) dividing a B-cell, (b) merging four successive B-cells in the same parent cell.

the longer sink trajectory (the longer staying time of sink) the cell needs in the next round. In order to change the staying time of the mobile sink in a B-cell, the sink trajectory in the B-cell can be adjusted by dividing the B-cell into smaller sub-cells or merging it with the other B-cells in its parent cell.

To judge whether a B-cell should be divided or merged, two data amount thresholds are set: the maximum data amount collecting threshold for it and the minimum data amount collecting threshold for its smallest parent cell.

For a B-cell Cb with side length l_{Cb}, the maximum data amount collecting threshold for it is denoted by $F1(Cb)$ which can be calculated as follows:

$$F1(Cb) = (l_{Cb}/v_0) \times DR_{\sin k} \tag{6}$$

Where v_0 is the movement speed of the mobile sink, DR_{sink} is the data receiving rate of the mobile sink, and l_{Cb} is also the length of sink trajectory in Cb in the current round.

If the data amount of B-cell Cb in the current round is greater than $F1(Cb)$, this B-cell Cb should be divided into four smaller sub-cells (as shown in Fig. 6(a)), therefore the sink trajectory in the next round in it will become longer and traverse the centers of these four smaller sub-cells.

For a parent cell C^* including four B-cells C^*-1 to C^*-4, the minimum data amount collecting threshold for it is denoted by $F2(C^*)$ which can be calculated as follows:

$$F2(C*) = (l_{C*}/v_0) \times DR_{\sin k} \tag{7}$$

Where l_{C^*} is the side length of the parent cell C^* as well as half length of the sink trajectory in C^* in the current round. If the data amount of cell C^* in the current round is less than $F2(C^*)$ and the data amount of each of the four B-cells C^*-1 to C^*-4 is less than $F1(C^*-1)$, these four B-cells C^*-1 to $C*-4$ should be merged into a new B-cell (as shown in Fig. 6(b)), therefore the sink trajectory in the next round in C^* will become shorter and traverse the center of the new B-cell.

It should be noted that, the data amount collecting threshold $F1(Cb)$ has higher priority in adjusting B-cell Cb, if the data amount of Cb in the current round is greater than $F1(Cb)$, but the data amount of its smallest parent cell C^* in the current round is less than $F2(C^*)$, this Cb should be divided into four smaller sub-cells rather than merged with the other B-cells in C^*.

Algorithm 1 Dynamic Adjustment Strategy for B-Cells

1. In a data gathering round:
2. when the mobile sink is traversing a B-cell Cb:
3. it communicates with the CA in Cb to get $DS(Cb)$ in the current round;
4. ***if*** $DS(Cb) > F1(Cb)$ **and** B-cellCb has not been divided or merged in this round
5. divide Cb into four new smaller cells (Cb-*1* to Cb-*4*) for the sink trajectory adjustment for the next round;
6. broadcast the message for electing the new CAs in the four new cells;
7. ***End if***
8. when the mobile sink is leaving a parent cell C^* including four B-cells C^*-1 to C^*-4:
9. ***if*** $\sum_{i=1}^{4} DS(C^* - i) < F2\,(C^*)$ **and** B-cells C^*-1 to C^*-4 have not been merged or divided in this round
10. merge the four B-cells C^*-1 to C^*-4 into a new B-cell for the movement trajectory adjustment for the next round;
11. broadcast the message for electing the new CA in the new B-cell;
12. ***End if***

With the above analysis, the algorithm for adjusting B-cells according to their data amounts is shown in Algorithm 1.

2) CELL ADJUSTMENT

Once the mobile sink has divided a cell or merged cells, it will broadcast the CA election message to the nodes in the new formed B-cell(s). The CA election message includes both the dynamic energy threshold and the cell name(s) of the new B-cell(s).

The name of a B-cell reveals the level it belongs to and its parent cell in each level. Thus, according to the name of a B-cell and the coordinates of the network center, the coordinates of the B-cell's center and its side length can be calculated by Algorithm 2.

The cell type of a cell which is decided before cell naming determines the sequence of the mobile sink traversing its sub-cells. There are four cell types that correspond to four types of sink traversing sequences respectively (denoted by *a, b, c,* and *d* in Algorithm 2). In Algorithm 2, a Hilbert map function is designed to check the corresponding sink traversing sequence of a B-cell's parent cell in each level according to the cell type of the B-cell's parent cell in each level. Each type of sink traversing sequence corresponds to a sequence of coordinate transformations (shown in Table 1) from the center coordinates of a B-cell's parent cell in level-$k-1$ to the center coordinates of the B-cell's parent cell in level-k. In Algorithm 2, a function called $T1$ is used to calculate the center coordinates of a B-cell's parent cell in level-k via the corresponding coordinate transformations which are related

Algorithm 2 Calculating the Center Coordinates and Side Length of a B-Cell

1. **Input**: the network size L, the coordinates of network center (x_0, y_0), the name cn of a cell Cb, the level lv of the cell Cb,
2. Hilbert_map = {
   'a': {1:('LB','d')}, 2:('LT','a'), 3:('RT','a'), 4:('RB','b')},
   'b': {1:('LB','a')}, 2:('RB','b'), 3:('RT','b'), 4:('LT','c')},
   'c': {1:('RT','d')}, 2:('RB','c'), 3:('LB','c'), 4:('LT','b')},
   'd': {1:('RT','c')}, 2:('LT','d'), 3:('LB','d'), 4:('RB','a')}};
3. **Output**: Cb's center coordinates (x_1, y_1), Cb's length len;
4. Put the digits of the Cb's name cn into an array $CN[]$ in sequence;
   //e.g. if cn=*C1-2-3*, it can set$CN[]$={1,2,3}.
5. $x_1 = x_0$, $y_1 = y_0$;
6. ***For*** $(i = 0; i < lv; i{+}{+})$
   //Calculate the center coordinates of the parent cells that Cb belongs to from level-*1* to level-lv until it finds the center coordinates of Cb.
7. $position = CN[i]$;
8. $direction, cell\_type$ = Hilbert_map $[cell\_type][position]$;
   //Look up the Hilbert_map with parameters $cell\_type$ and $position$ to get the movement direction and the cell_type for the next higher level parent cell that Cb belongs to.
9. $mlength = (1/2) * (L/2^{i+1})$;
   //Calculate the movement length to move to the next higher level parent cell that Cb belongs to.
10. x_1, y_1 = T1$(x_1, y_1, direction, mlength)$;
    //The function T1() is used to transform the coordinates (x_1, y_1) with $mlength$ and $direction$ (c.f. Table 1.) to get the center coordinates of the next higher level parent cell that the Cb belongs to.
11. ***End for***
12. $len = L/2^{lv}$; *//Calculate the side length of Cb*

to the sink traversing sequence of the B-cell's parent cell in level-$k{-}1$.

Once the center coordinates (x_1, y_1) and the side length len of a B-cell have been obtained, the specific scope of the B-cell could be calculated as follows:

$$\begin{cases} x \le x_1 + \dfrac{1}{2} \times len \\ x \ge x_1 - \dfrac{1}{2} \times len \end{cases} \quad and \quad \begin{cases} y \le y_1 + \dfrac{1}{2} \times len \\ y \ge y_1 - \dfrac{1}{2} \times len \end{cases} \tag{8}$$

When receiving a CA election message, a node can calculate the specific scope(s) of the B-cell(s) included in the message by Algorithm 2. Then, it can compare the scope(s) with its own location to find out which B-cell it belongs to and join in the CA election in the B-cell.

TABLE 1. Symbol list for directions.

Symbols	Meanings	Coordinate Transformations
'LT'	Left Top	$x = x - mlength$, $y = y + mlength$
'LB'	Left Bottom	$x = x - mlength$, $y = y - mlength$
'RT'	Right Top	$x = x + mlength$, $y = y + mlength$
'RB'	Right Bottom	$x = x + mlength$, $y = y - mlength$

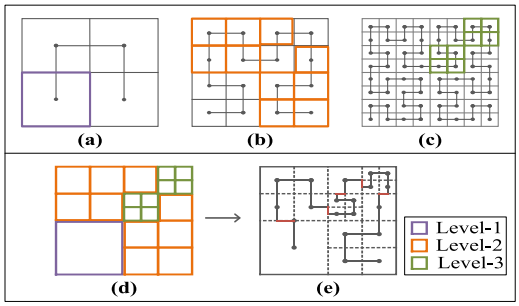

FIGURE 7. An example for the sink trajectory construction after cell adjustment : (a) basic *1*-order Hilbert curve; (b) basic *2*-order Hilbert curve; (c) basic *3*-order Hilbert curve; (d) adjusted B-cells in the network; (e) an updated sink trajectory.

3) TRAJECTORY ADJUSTMENT

After the cell adjustment, the mobile sink should adjust its trajectory for the next round in the new formed cells accordingly. To simplify the explanation, Fig. 7 provides an example to illustrate how to construct the sink trajectory. Fig. 7(d) shows the adjusted B-cells in the network that include B-cells in level-*1*, level-*2* and level-*3*. In order to construct the trajectory among these adjusted B-cells, the level-*1* B-cells (the purple cells), the level-*2* B-cells (the orange cells), and the level-*3* B-cells (the green cells) are filled by the basic *1*-order Hilbert curves (shown in Fig. 7(a)), the basic *2*-order Hilbert curves (shown in Fig. 7(b)), and the basic *3*-order Hilbert curves (shown in Fig. 7(c)), respectively. The updated sink trajectory for the adjusted B-cells in Fig. 7(d) is shown in Fig. 7(e).

At last, due to the combination of Hilbert curves with different orders in the network, the updated sink trajectory may be not continuous. Hence, the method in [4] is utilized to solve the sink trajectory connection problem on the borders of two adjacent cells with different levels in this work and make the whole sink trajectory continuous.

C. HYBRID ROUTING METHOD

In this section, a hybrid routing method is designed, in which, the transmission mode of a node can be determined according to the size of its B-cell. Fig. 8 shows the maximum required transmission ranges for nodes in B-cells with three different levels.

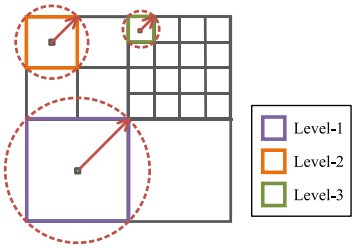

FIGURE 8. The maximum required transmission ranges for nodes in B-cells with three different levels.

Algorithm 3 The Hybrid Routing Method

1. In each B-cell:
2. CA calculates the maximum required transmission range r_t in its B-cell;
3. ***if*** (communication mode == cluster mode)
4. ***if*** ($r_t < 4r_{threshold}$)
5. CA broadcasts the *communication mode altering* message to change the communication mode to single-hop mode;
6. Nodes change their communication mode to single-hop mode;
7. Nodes transmit their sensing data to the CA directly;
8. ***end if***
9. ***else if*** (communication mode == single-hop mode)
10. ***if*** ($r_t >= 4r_{threshold}$)
11. CA broadcasts the *communication mode altering* message to change the communication mode to cluster mode;
12. Nodes change their communication mode to cluster mode;
13. Nodes begin to form clusters and elect Cluster Heads (CHs);
14. Nodes transmit their sensing data to their CHs;
15. CHs relay these data to the CA;
16. ***end if***
17. ***End if***.

From Fig. 8, it can be seen that, the cell in higher level has smaller cell size, and thus the maximum required transmission range in it is shorter. The maximum required transmission range r_t in a B-cell Cb can be calculated by (9), where L is the network size (side length), lv is the level of Cb.

$$r_t = \sqrt{2}L/2^{1+lv} \tag{9}$$

The proposed hybrid routing method is presented in Algorithm 3. In the routing method, each CA calculates the maximum required transmission range in its B-cell. If the maximum required transmission range in a B-cell is equal or higher than four times of a predetermined transmission range threshold $r_{threshold}$, the nodes in this B-cell use cluster mode to communicate with their CA, otherwise, they use single-hop mode.

The CAs in the adjusted B-cells need to calculate the maximum required transmission ranges in their B-cells and adjust the communication modes in their B-cells according to Algorithm 3, then inform the nodes in their B-cells of the adjusted communication modes.

TABLE 2. Simulation parameters.

Parameters	Values
Network size (L)	800m×800m
Number of sink	1
Movement speed of sink (v_0)	2 m/s
Maximum transmission range (r_{max})	100 m
Predetermined transmission range threshold in hybrid routing method ($r_{threshold}$)	25m
MAC	802.11
Initial energy of nodes (E)	10 J
Data receiving rate of sink (DR_{sink})	200b/s

TABLE 3. The data generating rates for three types of nodes.

Node Types	Type 1	Type 2	Type 3
Data Generating Rates	1kb/s	2kb/s	1.5kb/s

V. PERFORMANCE EVALUATION

In this section, our data gathering scheme is evaluated via simulations conducted in OMNeT++ 4.6 with the INET framework 3.3.0 [30].

In the simulations, the mobile sink is required to record the packet delivery ratio and the energy consumption rate of each node, a node N_i's energy consumption rate can be calculated by (10), where E_i is the energy that N_i needs for sending one bit to its CA, and E_0 is the energy that a node needs to send one bit to another node using the maximum transmission range r_{max} by single hop transmission mode.

$$\rho_i = E_i/E_0 \tag{10}$$

Via the simulations, the performances including the packet delivery ratio and the average energy consumption rate are compared between the data gathering scheme in [4] (denoted by *D-scheme*) and our scheme (denoted by *A-scheme*). Simulation parameters are shown in Table 2.

A. PERFORMANCE COMPARISON RELATED TO DIVERSITY OF DATA GENERATING RATE

In this section, performances in *D-scheme* and *A-scheme* are compared in two different scenarios: scenario 1 and scenario 2. In scenario 1, the data generating rates of all nodes are *1.5kb/s*. In scenario 2, there are three types of nodes with different data generating rates shown in Table 3 and the numbers of the three types of nodes are equal. In both of scenario 1 and scenario 2, the data generating rates of nodes are set constant, but the total number of nodes is set varying with time.

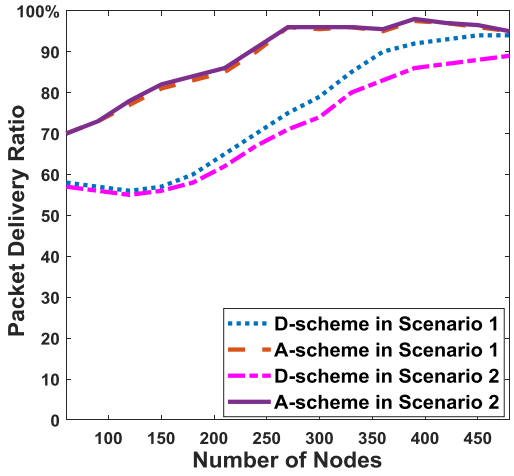

FIGURE 9. The packet delivery ratios in scenarios 1 and 2.

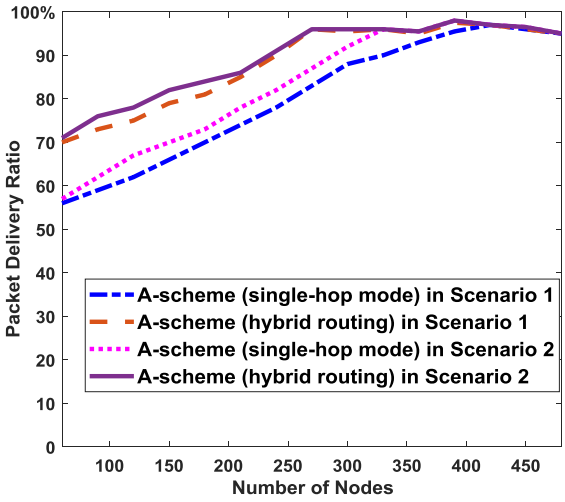

FIGURE 10. The effect of hybrid routing method on packet delivery ratios in scenarios 1 and 2.

TABLE 4. The highest curve orders in the simulations of scenarios 1 and 2.

Scenarios	Number of Nodes	*D-scheme*	*A-scheme*
1	60	1	1 (in cluster mode)
2	60	1	1 (in cluster mode)
1	120	1	1 (in cluster mode)
2	120	1	2 (in cluster mode)
1	240	2	2(in cluster mode)
2	240	2	3
1	360	3	3
2	360	3	3
1	480	3	3
2	480	3	4

1) COMPARISON OF PACKET DELIVERY RATIOS IN SCENARIOS 1 AND 2

The packet delivery ratios of *D-scheme* and *A-scheme* in scenarios 1 and 2 are shown in Fig. 9. From which, it can be seen that, when the node number is greater than 120, the packet delivery ratios in both of *D-scheme* and *A-scheme* increase with the growth of node number no matter in scenario 1 or 2, this is because, as the node number increases, the highest curve orders in the two schemes increase (the highest curve orders of sink trajectories in the simulations of scenarios 1 and 2 are shown in Table 4), so that their sink trajectories become longer and their average transmission distances for packets become shorter.

Fig. 9 shows that, the data delivery ratio of *A-scheme* is always higher than that of *D-scheme* no matter in scenario 1 or 2. In scenario 1 without the diversity of data generating rate, the difference between the packet delivery ratios in *D-scheme* and *A-scheme* is greater when the node number is less than 360, this is because, at this situation, the highest curve orders in *D-scheme* and *A-scheme* are less than 3, some nodes in *D-scheme* cannot communicate with the mobile sink and thus suffer a low packet delivery ratio, but the nodes in *A-scheme* can communicate with CAs via cluster mode.

In scenario 2, except for the single-hop transmission in *D-scheme*, the other reason for the lower data delivery ratio of *D-scheme* is that the *D-scheme* lacks the adaptability to the diversity of data generating rate, because it may happen that, in *D-scheme*, some cells have low node densities but high generated data amounts, thus their sink trajectories are not long enough to collect all of their data.

The simulation results of *D-scheme* in Fig. 9 show that, the packet delivery ratio of *D-scheme* in scenario 1 is higher than that in scenario 2, and with the increase of node number, the gap between the packet delivery ratios of *D-scheme* in scenarios 1 and 2 becomes greater, which can be explained by that, in scenario 2, when the node number is greater, the effect brought by the diversity of generating rate to impair the packet delivery ratio becomes greater.

Furthermore, the simulation results of *A-scheme* in Fig. 9 show that, the packet delivery ratio of *A-scheme* in scenario 2 is close to that in scenario 1, this means that the *A-scheme* has good adaptability to the diversity of data generating rate and thus contributes to the packet delivery ratio promotion in the heterogeneous sensing WSNs.

In order to evaluate the effect of hybrid routing method on the packet delivery ratio of *A-scheme*, the packet delivery ratios in *A-schemes* with single-hop transmission mode and hybrid routing method are compared in scenarios 1 and 2, and the comparison results are shown in Fig. 10.

Fig. 10 shows that, when the node number is less than 360 in scenario 1 and less than 240 in scenario 2, the packet delivery ratio in *A-scheme* with hybrid routing scheme is apparently higher than that in *A-scheme* with single-hop

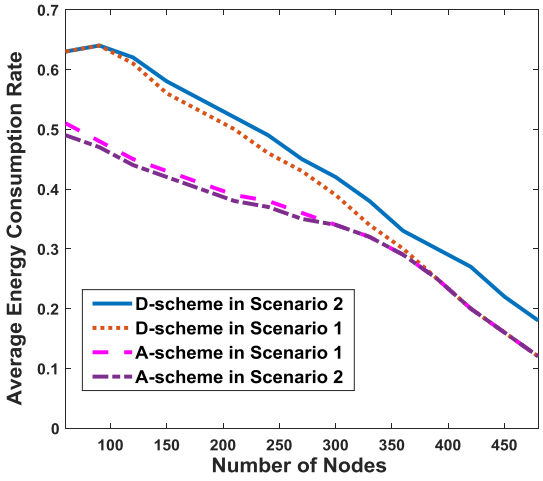

FIGURE 11. The average energy consumption rates in scenarios 1 and 2.

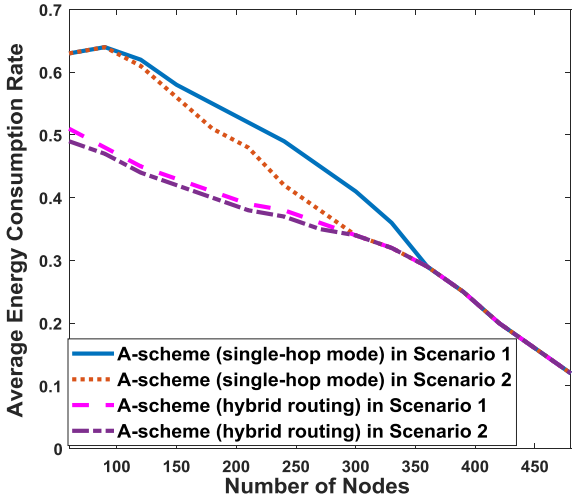

FIGURE 12. The effect of hybrid routing method on average energy consumption rates in scenarios 1 and 2.

transmission mode, this is because, in these situations, the highest curve orders of sink trajectories are less than 3, some nodes in network cannot communicate with their CAs directly, and the hybrid routing method is beneficial to promote their packet delivery ratios.

2) COMPARISON OF AVERAGE ENERGY CONSUMPTION RATES IN SCENARIOS 1 AND 2

The comparison of average energy consumption rates in scenarios 1 and 2 is shown in Fig. 11, from which it can be seen that, the average energy consumption rates in both *D-scheme* and *A-scheme* decrease with the growth of node number no matter in scenario 1 or 2, the reason is that, as the node number increases, the highest curve orders in the two schemes increase, so that their average transmission distances for packets become shorter.

In scenario 1, via theoretical analysis, it can be inferred that, if the node number is less than 360 (the highest curve orders in both *A-scheme* and *D-scheme* are less than 3), *A-scheme* will have shorter average transmission distance for packets than *D-scheme*, due to using the cluster mode in its hybrid routing method, and thus it will have lower average energy consumption rate than *D-scheme*. The theoretical inference is verified exactly by simulation results in scenario 1 shown in Fig. 11.

Fig. 11 also shows that, in scenario 2 with the diversity of data generating rate, *A-scheme* still has lower average energy consumption rate than *D-scheme,* this is caused by two reasons: 1) *A-scheme* supports cluster mode, and thus it has shorter average transmission distance when its highest curve order is less than 3; 2) *A-scheme* can change the length of sink trajectory in a cell according to the generated data amount of the cell, and thus if a cell has a greater generated data amount, it will has shorter average transmission distance. Conversely, *D-scheme* suffers higher average energy consumption rate for its single-hop transmission and lacking of the adaptability to the diversity of data generating rate.

The simulation results of *D-scheme* in Fig. 11 show that, the average energy consumption rate of *D-scheme* in scenario 2 is higher than that in scenario 1, and with the increase of node number, the gap between the average energy consumption rates of *D-scheme* in scenarios 1 and 2 becomes greater, this is because, in scenario 2, as the node number raises, the effect brought by the diversity of generating rate to increase average energy consumption rate becomes greater.

Furthermore, the simulation results of *A-scheme* in Fig. 11 show that, the average energy consumption rate of *A-scheme* in scenario 2 is close to that in scenario 1, this also proves that *A-scheme* has good adaptability to the diversity of data generating rate in the network.

In order to evaluate the effect of hybrid routing method on the average energy consumption rate of *A-scheme*, the average energy consumption rates in *A-schemes* with single-hop transmission mode and hybrid routing method are compared in scenarios 1 and 2, and the comparison results are shown in Fig. 12.

From Fig. 12, when the node number is less than 360 in scenario 1 and less than 240 in scenario 2, the average energy consumption rate in *A-scheme* with hybrid routing scheme is apparently lower than that in *A-scheme* with single-hop transmission mode, this is because, in these situations, the highest curve orders of sink trajectories are less than 3, the average transmission distance for packets in *A-scheme* with single-hop transmission mode is greater than that in *A-scheme* with hybrid routing method.

Because the average energy consumption rate in *A-scheme* is lower than that in *D-scheme, A-scheme* has longer network life than *D-scheme* especially in scenario 2, which is exactly verified by the simulation results in Fig. 13. In *A-scheme*, the hybrid routing method can reduce average energy consumption rate and thus it is beneficial for prolonging the network life, which is also proved by the simulation results in Fig. 14.

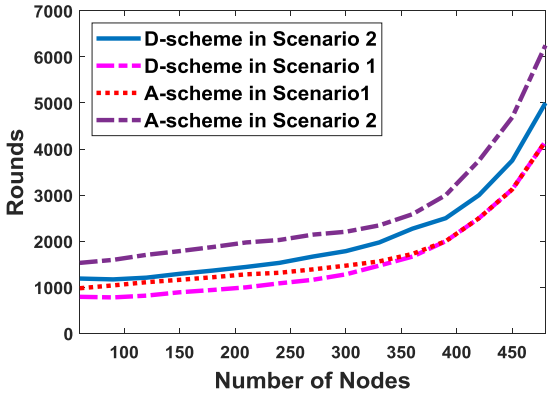

FIGURE 13. The network life in scenarios 1 and 2.

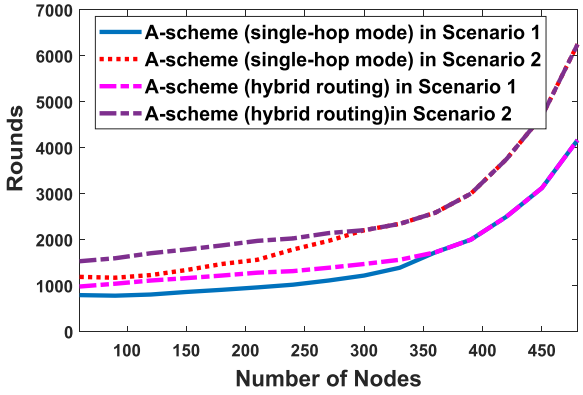

FIGURE 14. The effect of hybrid routing method on network life in scenarios 1 and 2.

B. PERFORMANCE COMPARISON RELATED TO DIVERSITY OF OPERATING MODE

In this section, performances in *D-scheme* and *A-scheme* are compared in two different scenarios: scenario 3 and scenario 4. The numbers of nodes are set to 240 in scenario 3 and 480 in scenario 4, separately. In both of the scenarios, three kinds of nodes with different types of operating modes (shown in Fig. 15) are distributed randomly in the network, the numbers of the three kinds of nodes are equal. In the simulations of scenarios 3 and 4, the average packet delivery ratios and the energy consumption rates in rounds of $12i+1$, $12i+3$, and $12i+7$ ($i=0, 1, 2, 3, 4\ldots.$) are recorded and calculated to evaluate the performance change related to the diversity of the operating mode.

The packet delivery ratios of *D-scheme* and *A-scheme* in scenarios 3 and 4 are shown in Fig. 16. The average energy consumption rates of *D-scheme* and *A-scheme* in scenarios 3 and 4 are shown in Fig. 17. The highest curve orders of the two schemes in both scenarios are shown in Table 5, and the sink trajectories of *D-scheme* and *A-scheme* in both scenarios are shown in Fig. 18.

From the simulation results in scenario 3, it can be seen that, as the number of working nodes increases, both of the packet delivery ratio and the average energy consumption rate in *D-scheme* almost keep consistent, which results from

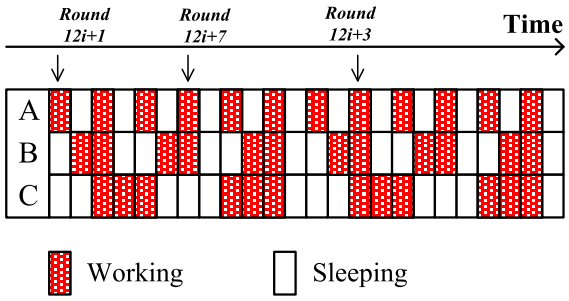

FIGURE 15. The schedule tables for three types of operating modes in the simulations of scenarios 3 and 4.

TABLE 5. The highest curve orders in the simulations of scenarios 3 and 4.

Rounds	Number of Nodes	*D-scheme*	*A-scheme*
$12i+1$	240	2	1
$12i+7$	240	2	2
$12i+3$	240	2	3
$12i+1$	480	2	3
$12i+7$	480	2	3
$12i+3$	480	2	4

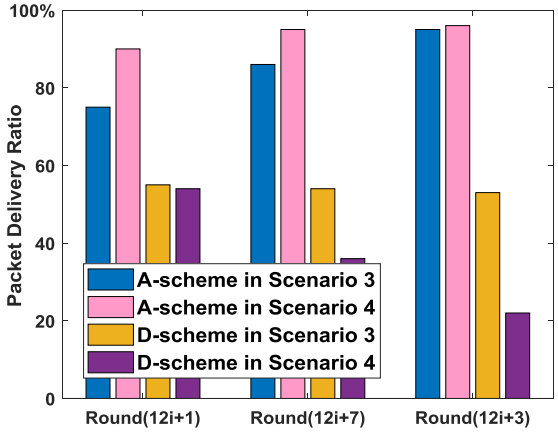

FIGURE 16. The packet delivery ratios in scenarios 3 and 4.

that, in *D-scheme* in scenario 3, when the node number and node density keep the same, the highest curve order of sink trajectory also keeps the same.

From the simulation results in scenario 4, it can be seen that, as the number of working nodes increases, the average energy consumption rate in *D-scheme* almost keeps consistent, but the packet delivery ratio in *D-scheme* decreases, which can be explained that, in scenario 4, *D-scheme* has the consistent average transmission rate due to its constant highest curve order of sink trajectory, but it cannot change the length of its sink trajectory to adapt to the increased data

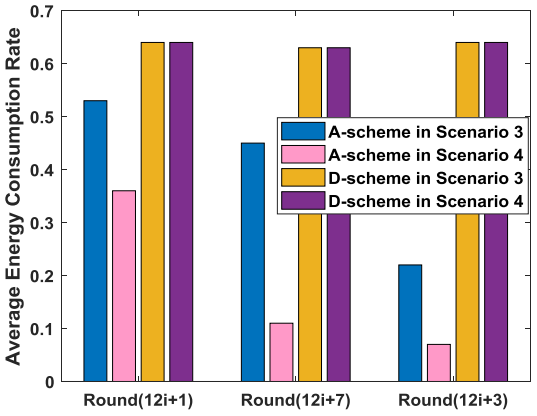

FIGURE 17. The average energy consumption rates in scenarios 3 and 4.

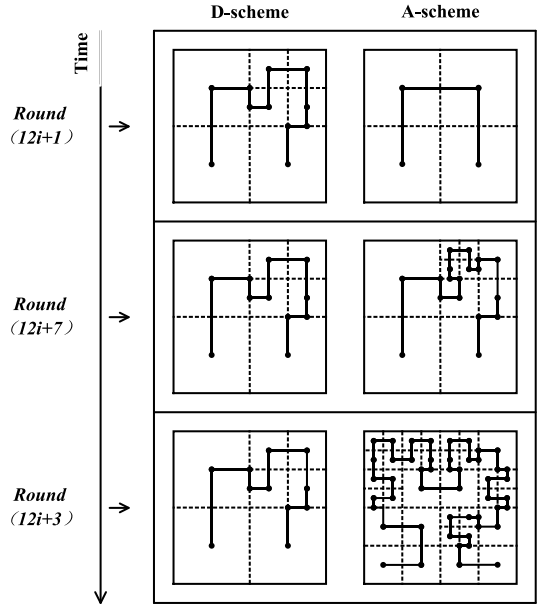

FIGURE 18. The sink trajectories in scenario 3.

amount caused by the increased number of working nodes, in other words, its constant sink trajectory is not long enough to collect all the increased data amount.

Fig. 16 and Fig. 17 show that, no matter in scenarios 3 or 4, the packet delivery ratio of *A-scheme* is always higher than that of *D-scheme*, and the average consumption rate of *A-scheme* is lower than that of *D-scheme*.

In both of scenarios 3 and 4, as the number of working nodes increases, the packet delivery ratio in *A-scheme* increases, but the average energy consumption rate in *A-scheme* decreases, this is because, in *A-scheme*, with the growth of working node number, the generated data mount in each cell increases, the highest curve order of sink trajectory increases accordingly (shown in Table 5 and Fig. 18), therefore the sink trajectory becomes longer, and thus the average energy consumption rate of nodes gets less and the packet delivery ratio gets greater.

Fig. 16 and Fig. 17 also show that, the packet delivery ratio of *A-scheme* in scenario 4 is higher than that in scenario 3, and the average energy consumption rate of *A-scheme* in scenario 4 is lower than that in scenario 3, which can be explained that, the highest curve order of sink trajectory in scenario 3 is less than that in scenario 4.

From the simulation results in scenarios 3 and 4, it can be seen that, compared with *D-scheme*, *A-scheme* has better adaptability to the diversity of operating mode, even in the network with large number of nodes.

VI. CONCLUSION

In this work, a data gathering scheme with a mobile sink using the controlled movement trajectory is proposed, which can track the data amount change in each network region and dynamically adjust the movement trajectory of sink in each network region according to the data amount tracking result. Further, the proposed scheme supports the hybrid routing method which can switch the transmission mode between single-hop mode and cluster mode. The simulation results verify that the proposed scheme has better performances on promoting the packet delivery ratio and reducing the energy consumption rate, and also has good adaptability to the diversities of data generating rate and operating mode, and thus it is beneficial for promoting the data gathering efficiency in the heterogeneous sensing WSNs.

In future work, we will further improve this scheme by absorbing experiences of the data collection method based on multiple sinks [31] and energy efficiency optimization [32], to make the scheme is applicable for large scale WSNs.

REFERENCES

[1] Y. Gu, F. Ren, Y. Ji, and J. Li, "The evolution of sink mobility management in wireless sensor networks: A survey," *IEEE Commun. Surveys Tuts.*, vol. 18, no. 1, pp. 507–524, 1st Quart., 2016.
[2] M. Perillo, Z. Cheng, and W. Heinzelman, "An analysis of strategies for mitigating the sensor network hot spot problem," in *Proc. IEEE Int. Conf. Mobile Ubiquitous Syst.*, Jul. 2005, pp. 474–478.
[3] C. Tunca, S. Isik, M. Y. Donmez, and C. Ersoy, "Distributed mobile sink routing for wireless sensor networks: A survey," *IEEE Commun. Surveys Tuts.*, vol. 16, no. 2, pp. 877–897, 2nd Quart., 2014.
[4] G. Yang, S. Liu, X. He, N. Xiong, and C. Wu, "Adjustable trajectory design based on node density for mobile sink in WSNs," *Sensors*, vol. 16, no. 12, 2016, Art. no. 2091.
[5] C. Zhu, V. C. M. Leung, K. Wang, L. T. Yang, and Y. Zhang, "Multi-method data delivery for green sensor-cloud," *IEEE Commun. Mag.*, vol. 55, no. 5, pp. 176–182, May 2017.
[6] S. Misra, S. Chatterjee, and M. S. Obaidat, "On theoretical modeling of sensor cloud: A paradigm shift from wireless sensor network," *IEEE Syst. J.*, vol. 11, no. 2, pp. 1084–1093, Jun. 2017.
[7] A. Wichmann and T. Korkmaz, "Smooth path construction and adjustment for multiple mobile sinks in wireless sensor networks," *Comput. Commun.*, vol. 72, pp. 93–106, Dec. 2015.
[8] A. C. Viana and M. D. de Amorim, "Sensing and acting with predefined trajectories," in *Proc. ACM HeterSanet*, 2008, pp. 1–8.
[9] S. Ghafoor, M. H. Rehmani, S. Cho, and S.-H. Park, "An efficient trajectory design for mobile sink in a wireless sensor network," *Comput. Electr. Eng.*, vol. 40, no. 7, pp. 2089–2100, 2014.
[10] J. Wang, J. Cao, S. Ji, and J. H. Park, "Energy-efficient cluster-based dynamic routes adjustment approach for wireless sensor networks with mobile sinks," *J. Supercomput.*, vol. 73, no. 7, pp. 3277–3290, 2017.
[11] A. Mehrabi and K. Kim, "Maximizing data collection throughput on a path in energy harvesting sensor networks using a mobile sink," *IEEE Trans. Mobile Comput.*, vol. 15, no. 3, pp. 690–704, Mar. 2016.

[12] A. Kinalis, S. Nikoletseas, D. Patroumpa, and J. Rolim, "Biased sink mobility with adaptive stop times for low latency data collection in sensor networks," *Inf. Fusion*, vol. 15, no. 1, pp. 56–63, 2014.
[13] X. Liu, H. Zhao, X. Yang, and X. Li, "SinkTrail: A proactive data reporting protocol for wireless sensor networks," *IEEE Trans. Comput.*, vol. 62, no. 1, pp. 151–162, Jan. 2013.
[14] G. Yang, H. Xu, X. He, G. Wang, N. Xiong, and C. Wu, "Tracking mobile sinks via analysis of movement angle changes in WSNs," *Sensors*, vol. 16, no. 4, 2016, Art. no. 449.
[15] G. Yang, L. Wang, L. Jiang, and X. He, "Biased trajectory dissemination of uncontrolled mobile sinks for event collection in wireless sensor networks," *Int. J. Distrib. Sensor Netw.*, vol. 12, no. 12, 2016, c no. 155014771668203.
[16] S. Sharma, D. Puthal, S. K. Jena, A. Y. Zomaya, and R. Ranjan, "Rendezvous based routing protocol for wireless sensor networks with mobile sink," *J. Supercomput.*, vol. 73, no. 3, pp. 1168–1188, 2016.
[17] C.-F. Wang, J.-D. Shih, B.-H. Pan, and T.-Y. Wu, "A network lifetime enhancement method for sink relocation and its analysis in wireless sensor networks," *IEEE Sensors J.*, vol. 14, no. 6, pp. 1932–1943, Jun. 2014.
[18] L. He, J. Pan, and J. Xu, "A progressive approach to reducing data collection latency in wireless sensor networks with mobile elements," *IEEE Trans. Mobile Comput.*, vol. 12, no. 7, pp. 1308–1320, Jul. 2013.
[19] A. Kaswan, K. Nitesh, and P. K. Jana, "Energy efficient path selection for mobile sink and data gathering in wireless sensor networks," *AEU-Int. J. Electron. Commun.*, vol. 73, pp. 110–118, Mar. 2016.
[20] C. Zhu, S. Zhang, G. Han, J. Jiang, and J. J. P. C. Rodrigues, "A greedy scanning data collection strategy for large-scale wireless sensor networks with a mobile sink," *Sensors*, vol. 16, no. 9, 2016, Art. no. 1432.
[21] C. Zhu, S. Wu, G. Han, L. Shu, and H. Wu, "A tree-cluster-based data-gathering algorithm for industrial WSNs with a mobile sink," *IEEE Access*, vol. 3, pp. 381–396, 2015.
[22] H. Salarian, K.-W. Chin, and F. Naghdy, "An energy-efficient mobile-sink path selection strategy for wireless sensor networks," *IEEE Trans. Veh. Technol.*, vol. 63, no. 5, pp. 2407–2419, Jun. 2014.
[23] J. Rao and S. Biswas, "Data harvesting in sensor networks using mobile sinks," *IEEE Wireless Commun.*, vol. 15, no. 6, pp. 63–70, Dec. 2008.
[24] Y. Bi, L. Sun, J. Ma, N. Li, I. A. Khan, and C. Chen, "HUMS: An autonomous moving strategy for mobile sinks in data-gathering sensor networks," *EURASIP J. Wireless Commun. Netw.*, vol. 2007, no. 1, p. 064574, 2007.
[25] M. Ma, Y. Yang, and M. Zhao, "Tour planning for mobile data-gathering mechanisms in wireless sensor networks," *IEEE Trans. Veh. Technol.*, vol. 62, no. 4, pp. 1472–1483, May 2013.
[26] N. Bulusu, J. Heidemann, and D. Estrin, "GPS-less low-cost outdoor localization for very small devices," *IEEE Pers. Commun.*, vol. 7, no. 5, pp. 28–34, Oct. 2000.
[27] D. Hilbert, "Ueber die stetige Abbildung einer Line auf ein Flächenstück," *Math. Ann.*, vol. 38, no. 3, pp. 459–460, 1970.
[28] H. V. Jagadish, "Linear clustering of objects with multiple attributes," in *Proc. ACM SIGMOD Int. Conf. Manage. Data ACM*, vol. 19, no. 2, 1990, pp. 332–342.
[29] T. Amgoth and P. K. Jana, "Energy-aware routing algorithm for wireless sensor networks," *Comput. Elect. Eng.*, vol. 41, no. 2, pp. 357–367, 2015.
[30] *INET Framework*. Accessed: Jun. 3, 2016. [Online]. Available: https://inet.omnetpp.org/
[31] L.-M. K. Ang, J. K. P. Seng, and A. M. Zungeru, "Optimizing energy consumption for big data collection in large-scale wireless sensor networks with mobile collectors," *IEEE Syst. J.*, vol. 12, no. 1, pp. 616–626, Mar. 2018.
[32] G. Wang, J. Wu, and Y. R. Zheng, "Optimum energy- and spectral-efficient transmissions for delay-constrained hybrid ARQ systems," *IEEE Trans. Veh. Technol.*, vol. 65, no. 7, pp. 5212–5221, Aug. 2014.

XINGYU HE received the Ph.D. degree in control theory and control engineering and the M.S. degree in system engineering from Tongji University in 2009 and 2017, respectively. She is currently a Lab Assistant with the Public Experiment Center, University of Shanghai for Science and Technology. Her research interests include wireless sensor networks, delay-tolerant networks, incentive scheme, swarm intelligence, and crowd sensing.

SHUAI LIU received the B.E. degree in communication engineering from the Nanjing University of Posts and Telecommunications in 2013. He is currently pursuing the master's degree in computer technology with the University of Shanghai for Science and Technology. His research interests include wireless sensor networks and computer networks.

GUISONG YANG received the Ph.D. degree in control theory and control engineering from Tongji University in 2013. He was a Research Scholar with Michigan State University from 2009 to 2011. He is currently an Associate Professor with the Department of Computer Science and Engineering, University of Shanghai for Science and Technology. His research interests include delay-tolerant and opportunistic networks, wireless sensor networks, and pervasive computing.

NAIXUE XIONG received the Ph.D. degrees in sensor system engineering and dependable sensor networks from Wuhan University and the Japan Advanced Institute of Science and Technology, respectively. He was with Georgia State University, Wentworth Technology Institution, and Colorado Technical University (a Full Professor for about five years) for 10 years. He is current an Associate Professor with the Department of Mathematics and Computer Science, Northeastern State University, Tahlequah, OK, USA. His research interests include cloud computing, security and dependability, parallel and distributed computing, sensor networks, and optimization theory.